The photophysics of solution processable semiconductors for applications in optoelectronic devices

Abdu-Aguye, Mustapha

DOI:
10.33612/diss.111696164

Chapter 5

Photophysical and electronic properties of bismuth-perovskite shelled lead sulphide quantum dots

In this work, we present a detailed photophysical study on two types of bismuth-based perovskite (MA_3BiI_6 and $MA_3Bi_2I_9$) shelled lead sulphide quantum dots (PbS QDs) using temperature-dependent photoluminescence (PL) spectroscopy between 5 K and 290 K and electrical measurements on field effect transistors (FETs). Our results reveal an increasing PL quantum yield and the activation of in-gap radiative states at lower temperatures. In addition, FET measurements at room temperature reveal electron-dominated transport with mobilities of around 10^{-3} $cm^2[Vs]^{-1}$, comparable to other perovskite-based shells for PbS QDs. These findings advance our understanding of perovskite shelled QD solids and point to the utility of these bismuth-based variants as contenders in photovoltaic and other optoelectronic applications.

This chapter is based on the publication:

M. Abdu-Aguye, D. Bederak, R. M. Dragoman, M. V. Kovalenko, W. Heiss, M. A. Loi. *J. Chem. Phys.*, **2019**, 151, 214702.

5.1 Introduction

Colloidal nanocrystals, or quantum dots (QDs) have attracted much attention over the past two decades for several important technological applications in fields as diverse as biological imaging[1], drug delivery[2], energy conversion[3,4] & storage[5] and optoelectronics. For optoelectronic applications, this is linked to the quantum-size effect that allows for tuning the bandgap[6] (and therefore absorption and emission) from the ultraviolet to the near-infrared spectral region as well as the ability to be processed through simple solution-based deposition methods for cost-effective and scalable mass production. Furthermore, they often exhibit superior stability compared to other solution-processable optoelectronic materials[7]. Among the many combinations of materials for QD-based optoelectronic devices, lead chalcogenides (PbX, X = S, Se, Te) are some of the most common due to their excellent carrier mobilities (linked to low carrier effective masses), well developed synthetic process and, photosensitivity in the (near) infra-red region coupled to a relatively large exciton Bohr radius (~ 18, 46 & 150 nm for PbS, PbSe & PbTe respectively); which enables them to retain quantum confinement even in relatively large particle sizes[8].

Decades of research into QD-based optoelectronics have led to great improvements of the synthetic techniques and to enhanced material quality, tuning of the electronic properties via surface modification or ligand exchange, and control of the formation of QD solids via a host of deposition techniques such as spin-coating, blade-coating or spray-coating. Surface ligands are a necessary addition during synthesis of colloidal QDs to stop growth and impart solubility, thus aiding long-term colloidal stability. However, these ligands are generally rather long and create a large potential barrier. Therefore, when charge carriers need to be extracted ligand exchange should be carried out to replace the native long insulating ligands such as oleic acid (OA) with shorter ones in order to improve the electronic coupling between adjacent QDs[9]. The first generation of QD-based optoelectronic devices featured post-deposition (or solid state) ligand exchange with short (bidentate) molecules such as thiols (ethanedithiol – EDT, 3-mercaptopropionic acid – MPA), amines (butylamine – BA), metal thiocyanates *etc.* were used in electrochemical cells, field effect transistors, solar cells, and photodetectors[10–13]. However, rather large challenges, related to film shrinkage, and the torturous layer-by-layer (LbL) processing to obtain films of the desired thickness appeared very soon.

Recently, solution-based ligand exchange methods such as liquid phase transfer where the ligand dissolved in a polar solvent reacts with the surface of the QDs, leaving the pristine ligand behind in the non-polar phase and bringing the QDs to the polar phase have been reported by several groups[9,13–16]. These inks are desirable because a single deposition step can be used to obtain films of the desired thickness; also, these layers appear less prone to form cracks during solvent evaporation[17,18]. Ligands such as metal chalcogenide complexes, thiols, (pseudo)halides, metal halides and more recently with (hybrid) metal halide (ABX_3) ligands[19] have been reported. Besides, their chemical compatibility with the surface of Pb chalcogenides, the rise of metal halide ligands is linked partially to their excellent optical and electronic properties as standalone materials, and also to the several studies that have shown a good lattice match with chalcogenides QD materials, such as PbS[20]. Pb-based perovskites have been the most widely studied as ligands, but also other metal ion complexes based on Sn^{2+}, Mn^{2+} [21], In^{3+} [22], and Bi^{3+} [23,24] have also recently been studied as alternatives. Bi has been recently investigated as a metal ion that can be used to form interesting perovskite and perovskite-like materials[25–27].

Recently, Sytnyk and co-workers reported the preparation and characterization of high-quality 0D perovskite shelled PbS QDs featuring high carrier mobility, and excellent results in photoconductors applications. Their experiments on octahedral metal halide clusters: $(MA^+)_{(6-x)}\,[M^{(x+)}\,Hal_6]^{(6-x)-}$ with (MA = methylammonium, M^{x+} = Pb^{2+}, Bi^{3+}, Mn^{2+}, In^{3+}, and Hal = Cl, I) resulted in the MA_3BiI_6 coated PbS based devices having the best performance – an observation they attributed to the low lattice mismatch of ca. -1%, which resulted in the most efficient passivation. Interestingly, this same Bi-based ligand shelled QD displayed a full quenching of the photoluminescence (PL) when in solution. Which was interpreted as due to the formation of a staggered heterostructure between the PbS core and the $(BiI_6)^{3-}$ clusters[28]. This is in contrast with what has been reported for Pb-based perovskite shelled QDs, which display similar PL (peak position and lifetimes) to OA-capped QDs in solution[18]. In addition, the PbS inks using $(PbI_3)^-$ as ligand have shown very good performances as active materials in solar cells and field effect transistors[15,18,29,30]. For this reason, the surprising behaviour of the Bi-based PbS QD ligand warrants further investigation.

In this study, two Bi-shelled PbS QD inks were synthesised using a modified procedure from Sytnyk *et al.*[28]. These are expected to have composition MA_3BiI_6 and $MA_3Bi_2I_9$, the former was also studied by Sytnyk and co-workers, while the latter has not been reported earlier as a PbS ligand.

5.2 Experimental

5.2.1 Ink Preparation

The PbS QDs were synthesized in a similar manner as reported elsewhere[31]. Solution-state ligand exchange was performed by using a modified recipe from Sytnyk et al[28]. In a typical procedure, 50 mM ligand solution in 10 ml DMF was prepared by mixing MAI and BiI_3 in 3:1 ratio for MA_3BiI_6, or in 3:2 ratio for $MA_3Bi_2I_9$. In both cases, the ligand solution turns red upon stirring and heating at 100 ˚C on a hot-plate. After cooling, the ligand solution was mixed with 10 ml of hexane dispersion of oleate-capped PbS CQDs with concentration of about 5 mg/ml. The mixture was stirred until the CQDs are transferred into polar phase. Then the top phase was discarded and the polar phase was washed 3 times with 10 ml of hexane. The Bi-shelled PbS CQDs were then precipitated by addition of toluene and collected by centrifugation. The supernatant was removed and the CQDs were re-dispersed in either 2,6-difluoropyridine (DFP) or propylene carbonate (PC) to form a QD ink.

5.2.2 Absorption Spectroscopy

Absorption measurements were carried out on dilute inks in 2 mm path length quartz cuvettes; or on masked areas of thin films deposited by spin-coating on quartz substrates using a dual beam Shimadzu spectrophotometer (UV-3600). From the absorption peak position of the OA-capped PbS QDs (~ 849 nm), we estimate a particle size of approximately 2.7 nm[32].

5.2.3 Photoluminescence (PL) Spectroscopy

PL measurements were carried out by exciting (unwashed) blade-coated samples with the 2nd harmonic of a Ti:Sapphire resonator ($\lambda \approx 400$ nm). Measurements were carried out in transmission mode and spectra were collected through a monochromator with 30 lines/mm and recorded by an ANDOR InGaAs inline detector (iDUS-1700). The laser spot on the sample was focussed via a 15 cm focal length lens, resulting in a diameter of approximately 100 μm.

For power dependent measurements, a neutral density filter wheel was used to vary the excitation power on the sample; for temperature dependent measurements: a cryostat equipped with flow and temperature controllers (Oxford Instruments) was used with liquid helium. All recorded spectra were corrected for the response of the setup using a calibrated lamp.

5.2.4 Field Effect Transistor (FET) fabrication and measurement

The substrates for FETs consist of highly doped Si with thermally grown 230 nm SiO_2 as gate dielectric. Pre-patterned ITO/Au electrodes served as source and drain electrode and formed a channel of 1 cm width and 20 μm length. The substrates were cleaned by consecutive sonication in acetone and isopropanol, dried in an oven, and treated by oxygen-plasma for 3 minutes before QD film deposition. The QD film was deposited by spin coating the ink of ligand-exchanged QDs in 2,6-difluoropyridine (DFP) at 1000 rpm after which the films were washed with Methanol. The devices were annealed for 20 min at 120 °C after the fabrication and then measured with an Agilent E5262 semiconductor parameter analyzer. All transistor fabrication and measurements were performed in a nitrogen-filled glovebox.

5.3 Results and Discussion

Figure 5.1(a) shows a schematic representation of the phase-transfer ligand exchange process employed to make the inks, as well as the layouts of samples for PL spectroscopy and FET measurements. Figure 5.1(b,c) shows the absorption spectra of the Bi-based inks (in DFP) and thin films. We note that the Bi-based inks display a weaker excitonic peak compared to the OA-based reference sample. This (inhomogeneous) broadening of the excitonic peak is likely due to changes in the surface passivation upon OA removal which leads to a variation in shell thicknesses, furthermore the variation of the solvent and consequently of its' polarity (DFP has a dielectric constant of 107.8) can also explain this effect, as it has been observed by other authors[18,33]. When thin films of the QDs are cast onto quartz substrates, once again – the Bi-based samples do not display a clear excitonic peak, unlike the OA-based sample. In this case, the absence of the excitonic peak is expected to result from an increased dielectric constant of their environment and closer electronic coupling between adjacent QDs.[18,34]

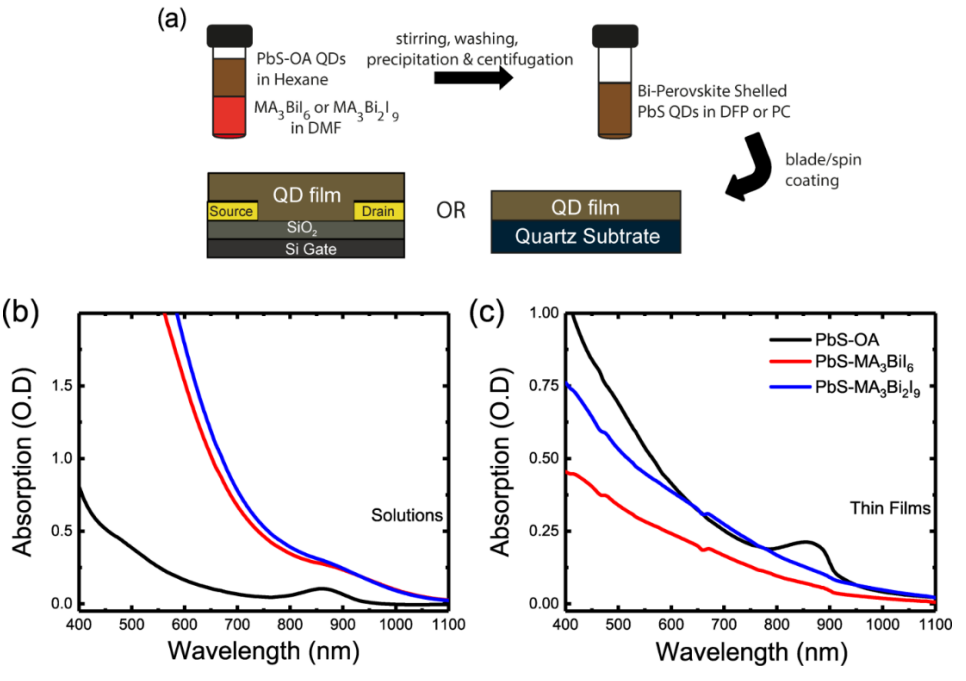

Figure 5.1: (a) Scheme of the phase transfer ligand exchange process. (b) Absorption spectra of the OA-capped PbS QD solution (in hexane) and Bi perovskite shelled PbS QDs in DFP. (c) Corresponding spectra of thin films on quartz substrates.

The photoluminescence spectra of the inks are shown in Figure 5.2(a). The Bi-perovskite shelled inks display broad peaks along with a tail at longer wavelengths, such broad spectra in solution are peculiar, in particular when compared with the parent OA-based sample which displays a narrow peak at 995 nm without any sub-bandgap emission or signs of extensive polydispersity. The dips in the solution PL spectra at ~ 1020 nm are due to absorption of the PL from the QDs by the solvent (DFP). While broad PL spectra have been reported for several ligands like TBAI, EDT and MPA[35–37], these apply to thin films and not to inks or solutions. This broad low energy features in the Bi-based samples seem to indicate clustering of the QDs driven by excess ligands. When cast into films via blade coating, the PL peaks for both Bi-based samples resemble the OA-based reference sample very closely (see Figure 5.2(b)); with an approximately 20 nm redshift relative to their main peaks

in solution, it should be noted that the films are unwashed. This leads to the question: what determines the large variation in the shape of the Bi-shelled samples?

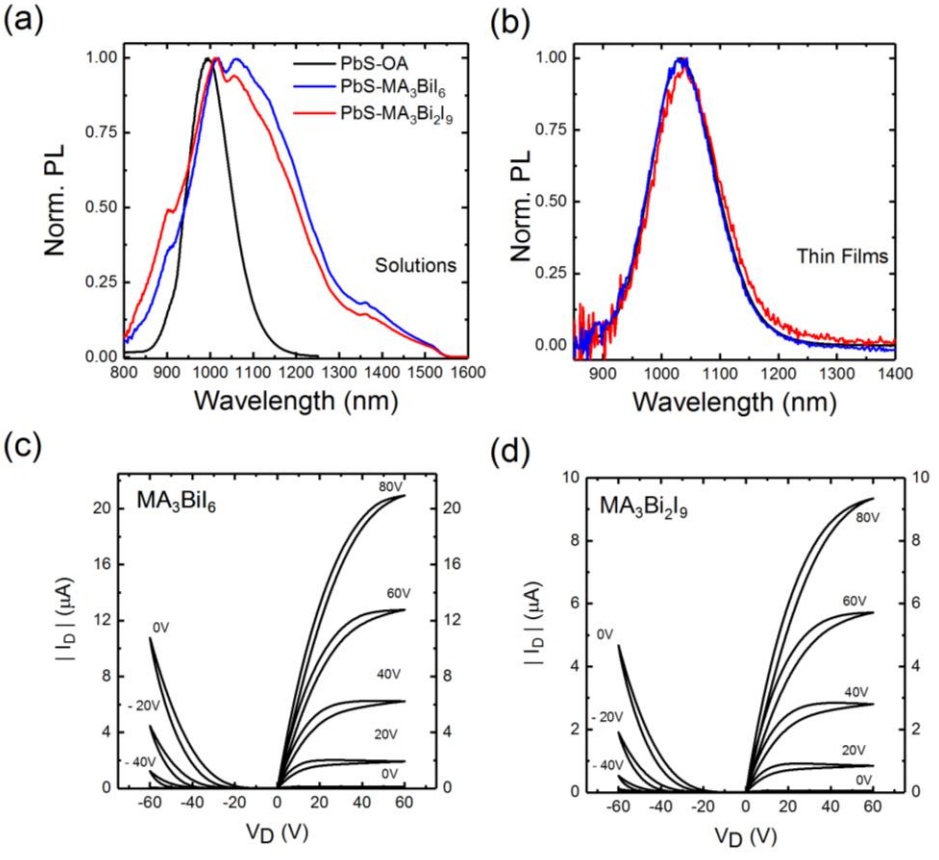

Figure 5.2: Steady-state photoluminescence spectra of OA-capped and Bi-perovskite shelled PbS QD solution/inks (a) and thin films on quartz (b); output curves for field effect transistors based on (c) MA_3BiI_6 and (d) $MA_3Bi_2I_9$ shelled QDs.

To gain more information about the electronic properties of the Bi-perovskite shelled QDs, field effect transistors were fabricated on Si/SiO_2 substrates, and the output characteristics are shown in Figures 5.2(c & d). The extracted linear mobility values(1.4×10^{-3} and 1.4×10^{-3} $cm^2[Vs]^{-1}$ for the $[BiI_6]^{3-}$ and $[Bi_2I_9]^{3-}$ shelled QDs respectively), although lower than recent records for LbL PbS QD FETs[38], are encouraging first results for Bi-perovskite shelled PbS-QD thin films, and compare favourably with mobilities for other PbS inks such as those with ligands such as $MAPbI_3$, MPA and halides[18,39,40]. More importantly, these results confirm the removal of the native OA based ligands without which transport is essentially

impossible[41,42]. As can be seen by the higher drain currents in the n-channel from the output curves, the FETs display more electron-dominant transport. This is also reflected in the transfer curves depicted in Figure S5-3.

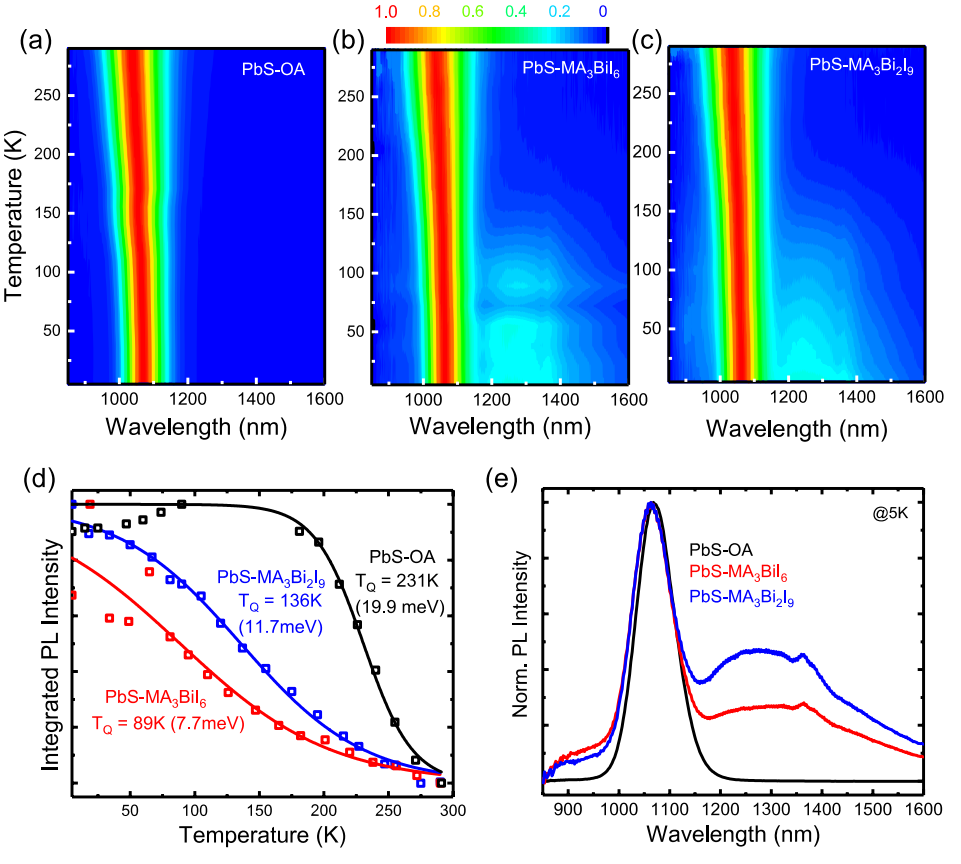

Figure 5.3: Temperature dependent PL plots of (a) OA-capped PbS QDs, (b) PbS-MA_3BiI_6 QDs and (c) PbS-$MA_3Bi_2I_9$ QDs. (d) Integrated PL intensity vs. temperature plots for the OA and Bi-shelled PbS QDs fit to equation (5.1) with obtained values for the quenching temperature, T_Q and (e) Representative PL spectra of the samples at 5 K.

Temperature-dependent PL measurements are an important tool to gauge more physical information about QD solids. Figure 5.3(a) shows the strong temperature dependence of the PL from reference thin films of OA-capped QDs. The PL at room temperature (RT) exhibits a single peak at ~1029 nm with a FWHM of 129 nm. When the temperature is decreased, the PL emission becomes stronger, as has been variously reported before in PbX QDs[43,44]. At 5 K it is already more than double in intensity and the FWHM has decreased to ~ 89 nm. Another consequence

of decreasing the temperature is a bathochromic shift of the emission from RT to 5K (1029 nm to 1068 nm), this red shifted PL emission can be explained as an interplay between the thermal expansion of the QDs described by a size-dependent temperature coefficient, temperature-mediated interactions between phonons and charge carriers as well as the effect of confinement energy on the effective masses of carriers[44,45]. The increasing PL intensity and decreasing FWHM at low temperature are a consequence of reduced electron-phonon scattering due to reduced number of lattice vibrations at low temperature which is known to result in quenching of excitons[34]. The evolution of the FWHM and peak position as a function of temperature is shown in Figure 5.4.

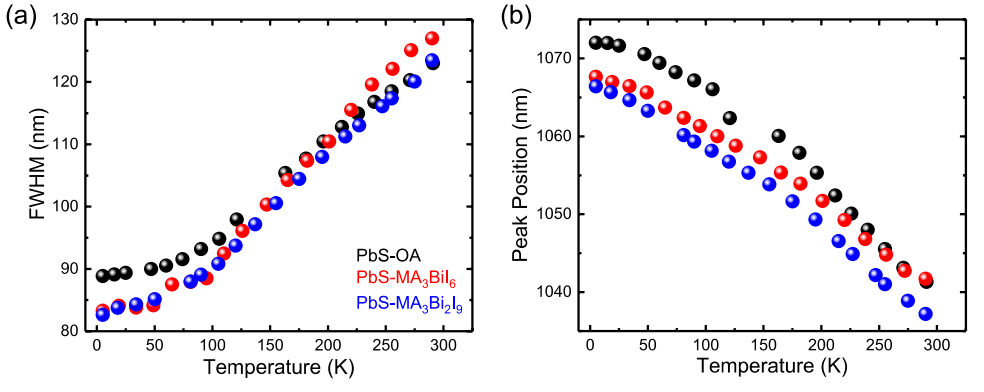

Figure 5.4: The (a) FWHM and (b) peak position of the PL emission as a function of temperature for the PbS-OA, PbS-MA_3BiI_6 and PbS-$MA_3Bi_2I_9$ samples.

For the Bi-perovskite capped PbS QD films, the temperature dependent PL spectra are shown in Figures 5.3(b & c) - with RT peak positions at 1038 nm and 1043 nm for the $[BiI_6]^{3-}$ and $[Bi_2I_9]^{3-}$ samples respectively; and FWHM values of 132 nm and 128 nm. Similar to the OA-based reference sample, there is a bathochromic shift of the PL as temperature decreases together with a corresponding increase in the PL intensity (by a factor of ~ 5 between RT and 5 K in both cases), i.e. a quenched PL is obtained as temperature goes up from 5 K. Temperature-mediated PL quenching is usually quantified in terms of a Boltzmann model[46]:

$$I_{PL}(T) = \frac{1}{1 + exp\,[(T - T_Q)/\varphi]} \qquad (5.1)$$

Where I_{PL} is the integrated PL intensity (normalized, in this case); T_Q and φ are fit parameters representing the quenching temperature and rate respectively. T_Q can be

interpreted as the temperature associated with thermal quenching of excitons; and φ represents a quenching rate associated with T_Q. In general, a higher T_Q is necessary for better stabilization of excitons and more efficient PL[26]. From the fits shown in Figure 5.3(d), we obtain T_Q values of 89 K, 136 K and 231 K, corresponding to thermal energies (required for the non-radiative quenching of excitons) (i.e. $k_B T_Q$) of 7.7 meV, 11.7 meV and 19.9 meV for the $[BiI_6]^{3-}$, $[Bi_2I_9]^{3-}$ and OA capped samples respectively. The next figure, 5.3(d), shows a comparison between the shapes of the PL of the samples at 5 K, as can be inferred from 5.3(b,c) the Bi-capped samples display a broad emission feature at lower energies than the main peak. This behaviour is all the more interesting since the same batch of OA-capped PbS QDs display very different behaviour when Pb-based perovskite ligands ($MAPbI_3$ and MA_4PbI_6) are used – see Figure S5-4 for their corresponding temperature-dependent PL spectra to contrast with Figures 5.3(a-c).

This important feature of the temperature dependent PL spectra of the Bi-perovskite capped thin films initially emerges below approximately 100 K. Similar behaviour has been observed in both thiol- (EDT, MPA) & I^--capped PbS QDs, and is attributed to radiative recombination from shallow below bandgap trap states [36,46,47]. Such an emission is absent in the reference OA-capped QD film, presumably because it passivates the QDs efficiently[48] – this can be seen from the PL shape, which remains unchanged at both 5 K and RT, (see supporting information Figure S5-1(a-c)). This indicates that the source of the trap states is the surface of the QDs. Furthermore, we can infer that these traps are induced by the ligand exchange process and that the Bi-shelled QDs are not well passivated.

Turning our attention to the Bi-based PbS QD films, we performed power dependent PL measurements at both RT and 5 K. The Bi-perovskite shelled samples display changing spectra as a function of excitation power, showing a trap-filling mechanism occurring at these temperatures as the excitation power is increased (see Figure S5-2(c-f)). Figure 5.5 shows a plot of the integrated PL intensity versus the excitation power density for the three samples both at room and low temperature. The slope of the measured data is the fit to a power law relation of form[49]:

$$I_{PL}(P) = \eta P^{\alpha} \qquad (5.2)$$

With I_{PL}, P, and α respectively representing the integrated PL intensity, excitation power density, and a recombination exponent. η represents an empirical "catch all"

term which encompasses the PL quantum yield, absorption, sample geometry, etc. The recombination exponent α, is generally expected to fall between 1 for excitonic recombination and 2 for bimolecular recombination between uncorrelated electron-hole pairs.

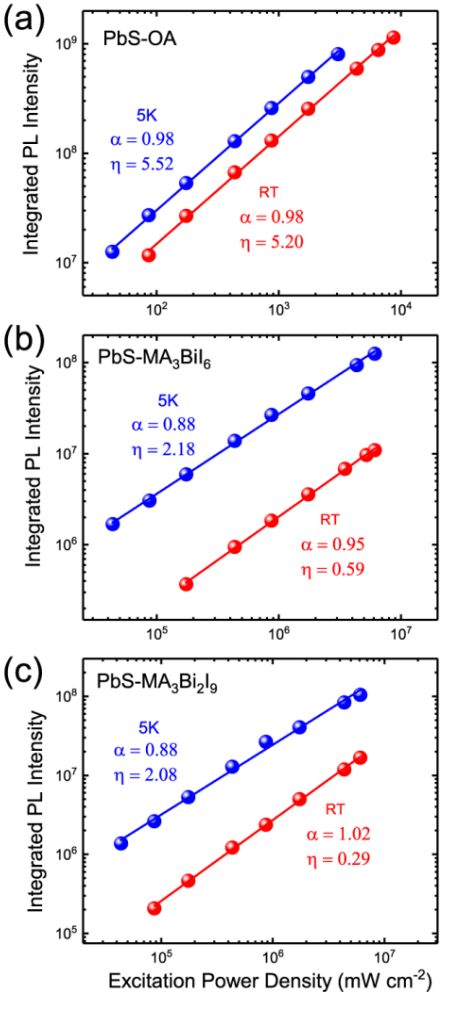

Figure 5.5: Integrated PL vs. excitation power density at 5 K and RT for (a) PbS-OA QDs (b) PbS-MA_3BiI_6 QDs and (c) PbS-$MA_3Bi_2I_9$ QDs; insets show the extracted values for α and η from equation (5.2).

It is important to note that the excitation power density for the Bi-shelled samples is over two orders of magnitude higher than that of the OA-capped one. Much higher PL signals from the reference OA-capped sample were obtained, which is

further evidence for the lower amount of non radiative recombination sites in the well passivated OA-sample. An additional important consideration is that the occurrence energy transfer has been reported in the case of OA-capped QDs[45], thus, in QDs with shorter ligands, energy transfer is expected to be more effective, increasing the probability of non-radiative recombination.

As mentioned above, the solid lines in the plots shown in Figure 5.5 represent the best-fit to equation 5.2. As expected, α for the OA-reference sample is approximately 1 at both 5 K and RT, and the η values remain both very similar (5.52 and 5.20, respectively) indicating a predominantly excitonic recombination mechanism with a slightly increased PL efficiency at 5 K compared to RT. For the Bi-based samples on the other hand, a few interesting differences can be seen: the first is that although the recombination mechanism remains excitonic in nature (α around 1), it is lower at 5 K (0.88 in both cases) than it is at RT (0.95 & 1.02 for $[BiI_6]^{3-}$ and $[Bi_2I_9]^{3-}$ respectively).

This is in good agreement with the earlier observations of the emergence of a broad emission feature below the bandgap at low temperatures which leads us to the conclusion that such below gap radiative states are indeed trap-like. At RT, such PL signals are absent, which reflects in a higher α value since the low temperature emission represents a loss mechanism to the mean excitonic emission peak. The second observation that can be made is that the η parameter varies significantly between RT and 5 K for both the $[BiI_6]^{3-}$ sample (0.59 & 2.18 at RT and 5 K respectively) and $[Bi_2I_9]^{3-}$ (0.29 & 2.08, ditto). This large difference (η is on a log scale, thus a difference of $\Delta\eta = 1$ represents an order of magnitude difference in PL efficiency, under the assumption that all changes are temperature dependent) strongly shows that the PL efficiency of the Bi-based samples is much lower than that of the OA-based reference films, especially at RT.

A similar sublinear power dependence ($\alpha < 1$) of the integrated PL of ligand-exchanged PbS films at low temperatures has been reported before[46,47]; such observations, together with the assertion of an increased carrier lifetime at low temperatures reported before for both PbS[50] and PbSe[43] QDs point towards either a redistribution of the excited state population from bright (highly radiative) exciton states to dark (relatively lower radiative) states or to a changing non-radiative decay rate with temperature. This harkens to the assertion of a strong sensitivity of the surface of the Bi-shelled PbS QDs to the quality of passivation as

seen in several studies with other passivating ligands, and implies that there is still much room for further development of these Bi-perovskite shelled QD solids.

5.4 Conclusion

We report herein FETs and PL measurements on Bi-shelled PbS inks and solids. Our PL measurements on thin films reveal the presence of sub-band gap radiative states which become visible at temperatures below ~ 100 K; an observation supported by previous studies on PbS-QDs. Using temperature dependent PL measurements, we obtain quenching temperatures (energies) of 231 K, 89 K, and 136 K for the PbS-OA, PbS-MA_3BiI_6 and PbS-$MA_3Bi_2I_9$ samples respectively. From power-dependent measurements, we show that the PL efficiency of the OA samples is much higher than the Bi-shelled ones – which suffer from traps; most likely formed at their surfaces during the phase-transfer ligand exchange process. Nevertheless, results from electrical measurements on FETs show the successful removal of the native-OA ligands, displaying electron dominated transport with modest mobilities of around 10^{-3} $cm^2[Vs]^{-1}$ – comparable to reported values for epitaxial Pb-based shelled samples. These results improve our understanding of Bi-perovskite shelled PbS QD solids, which are contenders for diverse optoelectronic applications such as absorber layers in solar cells and photodetectors.

5.5 Supporting Information

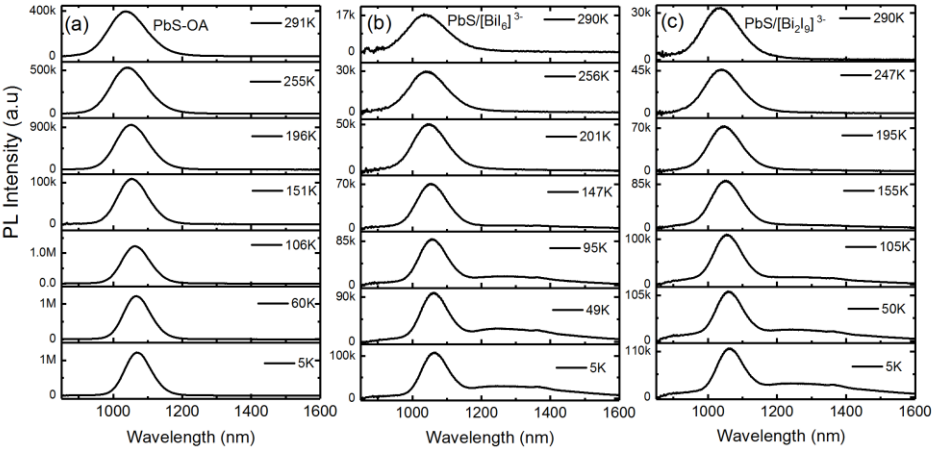

S-5. 1: PL emission of (a) PbS-OA, (b) PbS/$[BiI_6]^{3-}$ and (c) PbS/$[Bi_2I_9]^{3-}$ QDs at selected temperatures showing the spectral shape evolution as temperature is decreased from RT to 5 K.

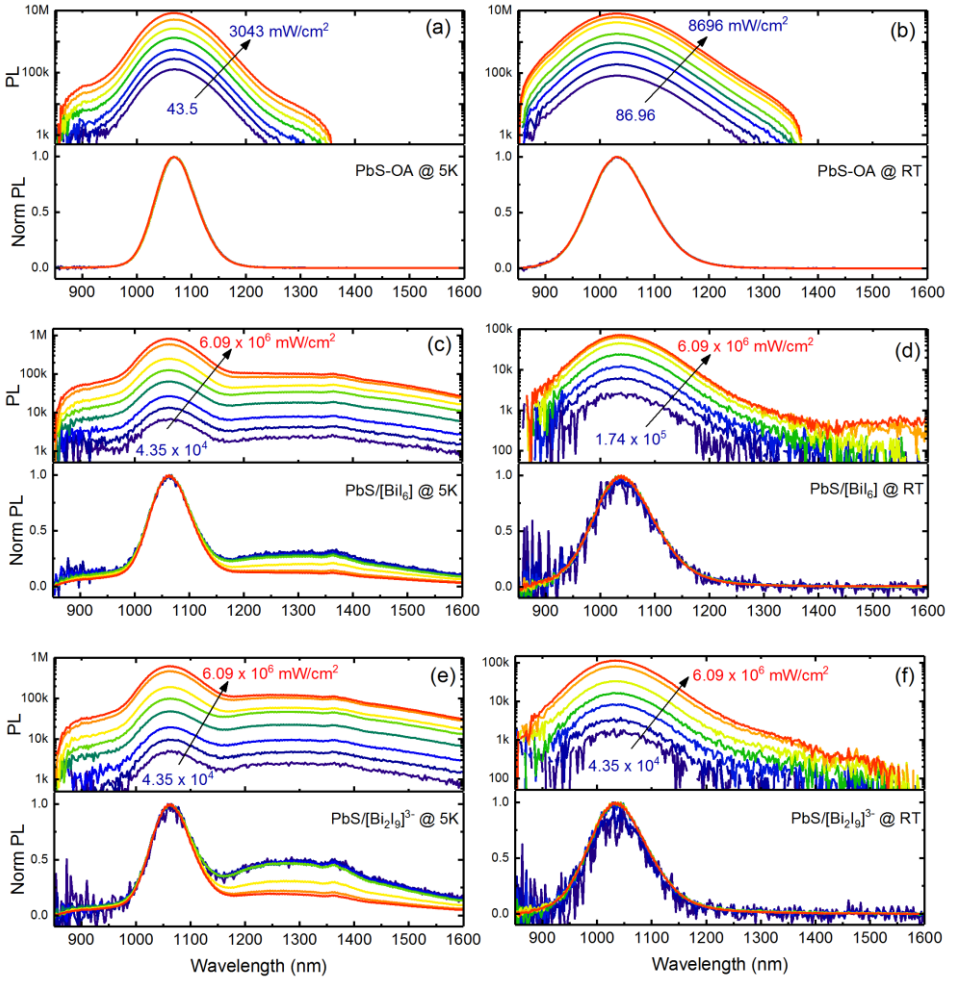

S-5. 2: Excitation Power Dependence of the PL spectra for PbS-OA (a, b), PbS/$[BiI_6]^{3-}$ (c, d) and PbS/$[Bi_2I_9]^{3-}$ (e, f) QDs at 5 K and RT respectively

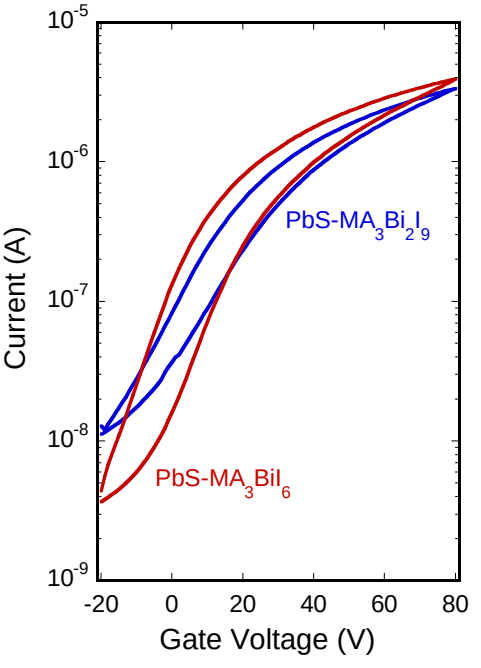

S-5. 3: Representative output curve for the FETs with the Bi-shelled samples measured at 5V.

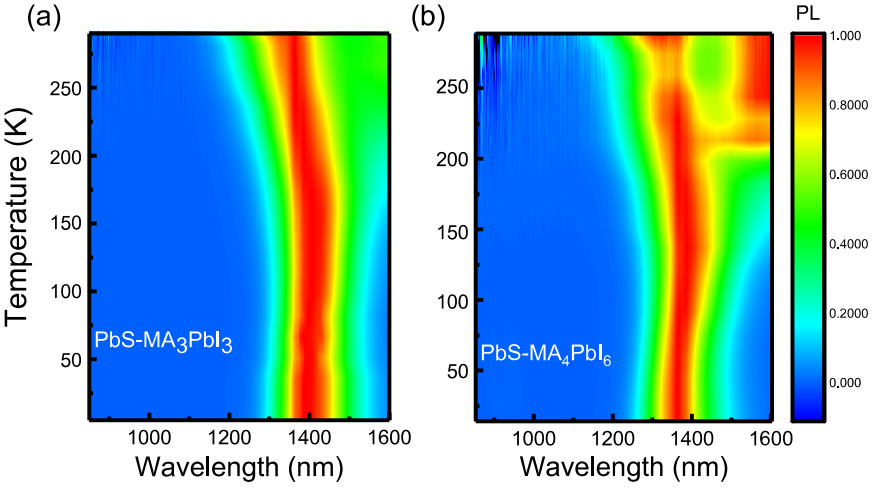

S-5. 4: Temperature dependence of PL spectra for (a) PbS-MAPbI$_3$ and (b) PbS-MA$_4$PbI$_6$.

References

[1] O. V. Salata, *J. Nanobiotechnology* **2004**, *2*, 3.

[2] C. E. Probst, P. Zrazhevskiy, V. Bagalkot, X. Gao, *Adv. Drug Deliv. Rev.* **2013**, *65*, 703.

[3] T. C. Harman, P. J. Taylor, M. P. Walsh, B. E. Laforge, *Science (80-.).* **2002**, *297*, 2229.

[4] G. H. Carey, A. L. Abdelhady, Z. Ning, S. M. Thon, O. M. Bakr, E. H. Sargent, *Chem. Rev.* **2015**, 12732.

[5] P. Wu, Y. Xu, J. Zhan, Y. Li, H. Xue, H. Pang, *Small* **2018**, *14*, 1.

[6] J. M. Luther, J. Gao, M. T. Lloyd, O. E. Semonin, M. C. Beard, A. J. Nozik, *Adv. Mater.* **2010**, *22*, 3704.

[7] A. P. Alivisatos, *Science (80-.).* **1996**, *271*, 933.

[8] H. Fu, S. W. Tsang, *Nanoscale* **2012**, *4*, 2187.

[9] A. T. Fafarman, W. Koh, B. T. Diroll, D. K. Kim, D. Ko, S. J. Oh, X. Ye, V. Doan-Nguyen, M. R. Crump, D. C. Reifsnyder, C. B. Murray, C. R. Kagan, *J. Am. Chem. Soc* **2011**, 15753.

[10] D. Yu, C. Wang, P. Guyot-Sionnest, *Science (80-.).* **2003**, *300*, 1277.

[11] D. V Talapin, C. B. Murray, *Science (80-.).* **2005**, *310*, 86.

[12] E. J. D. Klem, D. D. Macneil, P. W. Cyr, L. Levina, E. H. Sargent, *Appl. Phys. Lett* **2008**, *90*, 1.

[13] G. Konstantatos, I. Howard, A. Fischer, S. Hoogland, J. Clifford, E. Klem, L. Levina, E. H. Sargent, *Nature* **2006**, *442*, 180.

[14] D. N. Dirin, S. Dreyfuss, M. I. Bodnarchuk, G. Nedelcu, P. Papagiorgis, G. Itskos, M. V. Kovalenko, *J. Am. Chem. Soc.* **2014**, *136*, 6550.

[15] M. Liu, O. Voznyy, R. Sabatini, F. P. G. De Arquer, R. Munir, A. H. Balawi, X. Lan, F. Fan, G. Walters, A. R. Kirmani, S. Hoogland, F. Laquai, A. Amassian, E. H. Sargent, *Nat. Mater.* **2017**, *16*, 258.

[16] H. Aqoma, M. Al Mubarok, W. T. Hadmojo, E. Lee, T. Kim, T. K. Ahn, S. Oh, S. Jang, *Adv. Mater.* **2017**, *29*, 1.

[17] Q. Lin, H. J. Yun, W. Liu, H. J. Song, N. S. Makarov, O. Isaienko, T. Nakotte, G. Chen, H. Luo, V. I. Klimov, J. M. Pietryga, *J. Am. Chem. Soc.* **2017**, *139*, 6644.

[18] D. M. Balazs, N. Rizkia, H.-H. Fang, D. N. Dirin, J. Momand, B. J. Kooi, M. V Kovalenko, M. A. Loi, *ACS Appl. Mater. Interfaces* **2018**, *10*, 5626.

[19] H. Zhang, J. Jang, W. Liu, D. V. Talapin, *ACS Nano* **2014**, *8*, 7359.

[20] Z. Ning, X. Gong, R. Comin, G. Walters, F. Fan, O. Voznyy, E. Yassitepe, A. Buin,

S. Hoogland, E. H. Sargent, *Nature* **2015**, *523*, 324.

[21] R. A. Lalancette, N. Elliott, I. Bernal, *J. Cryst. Mol. Struct.* **1972**, *2*, 143.

[22] J. G. Contreras, F. W. B. Einstein, M. M. Gilbert, D. G. Tuck, *Acta Crystallogr.* **1977**, *030*, 1648.

[23] M. Lindsjö, A. Fischer, L. Kloo, *Zeitschrift fur Anorg. und Allg. Chemie* **2005**, *631*, 1497.

[24] L. M. Wu, X. T. Wu, L. Chen, *Coord. Chem. Rev.* **2009**, *253*, 2787.

[25] U. Dasgupta, B. Kundu, A. J. Pal, *Sol. RRL* **2018**, *1800012*, 1800012.

[26] M. Leng, Y. Yang, Z. Chen, W. Gao, J. Zhang, G. Niu, D. Li, H. Song, J. Zhang, S. Jin, J. Tang, *Nano Lett.* **2018**, *18*, 6076.

[27] A. H. Slavney, T. Hu, A. M. Lindenberg, H. I. Karunadasa, *J. Am. Chem. Soc.* **2016**, *138*, 2138.

[28] M. Sytnyk, S. Yakunin, W. Schöfberger, R. T. Lechner, M. Burian, L. Ludescher, N. A. Killilea, A. Yousefiamin, D. Kriegner, J. Stangl, H. Groiss, W. Heiss, *ACS Nano* **2017**, *11*, 1246.

[29] J. Peng, Y. Chen, X. Zhang, A. Dong, Z. Liang, *Adv. Sci.* **2015**, *3*, 1.

[30] Z. Yang, A. Janmohamed, X. Lan, F. P. García De Arquer, O. Voznyy, E. Yassitepe, G. H. Kim, Z. Ning, X. Gong, R. Comin, E. H. Sargent, *Nano Lett.* **2015**, *15*, 7539.

[31] M. A. Hines, G. D. Scholes, *Adv. Mater.* **2003**, *15*, 1844.

[32] I. Moreels, K. Lambert, D. Smeets, D. De Muynck, *ACS Nano* **2009**, *3*, 3023.

[33] T. Takagahara, *Phys. Rev. B* **1993**, *47*, 4569.

[34] K. Szendrei, M. Speirs, W. Gomulya, D. Jarzab, M. Manca, O. V Mikhnenko, M. Yarema, B. J. Kooi, W. Heiss, M. A. Loi, *Adv. Funct. Mater.* **2012**, 1598.

[35] G. W. Hwang, D. Kim, J. M. Cordero, M. W. B. Wilson, C. H. M. Chuang, J. C. Grossman, M. G. Bawendi, *Adv. Mater.* **2015**, *27*, 4481.

[36] M. J. Speirs, D. N. Dirin, M. Abdu-Aguye, D. M. Balazs, M. V. Kovalenko, M. A. Loi, *Energy Environ. Sci.* **2016**, 2916.

[37] L. Hu, A. Mandelis, Z. Yang, X. Guo, X. Lan, M. Liu, G. Walters, A. Melnikov, E. H. Sargent, *Sol. Energy Mater. Sol. Cells* **2017**, *164*, 135.

[38] A. G. Shulga, V. Derenskyi, J. M. Salazar-Rios, D. N. Dirin, M. Fritsch, M. V Kovalenko, U. Scherf, M. A. Loi, *Adv. Mater.* **2017**, *1701764*, 1.

[39] M. I. Nugraha, S. Kumagai, S. Watanabe, M. Sytnyk, W. Heiss, M. A. Loi, J. Takeya, *ACS Appl. Mater. Interfaces* **2017**, 18039.

[40] D. Bederak, D. M. Balazs, N. V. Sukharevska, A. G. Shulga, M. Abdu-Aguye, D. N. Dirin, M. V. Kovalenko, M. A. Loi, *ACS Appl. Nanomater.* **2018**, DOI 10.1021/acsanm.8b01696.

[41] D. V Talapin, J. Lee, M. V Kovalenko, E. V Shevchenko, *Chem. Rev.* **2010**, 389.

[42] R. Wang, Y. Shang, P. Kanjanaboos, W. Zhou, Z. Ning, E. H. Sargent, *Energy Environ. Sci.* **2016**, *9*, 1130.

[43] R. D. Schaller, S. A. Crooker, D. A. Bussian, J. M. Pietryga, J. Joo, V. I. Klimov, *Phys. Rev. Lett.* **2010**, *105*, 8.

[44] P. J. Roland, K. P. Bhandari, R. J. Ellingson, *J. Appl. Phys.* **2016**, *119*, 1.

[45] H. H. Fang, D. M. Balazs, L. Protesescu, M. V. Kovalenko, M. A. Loi, *J. Phys. Chem. C* **2015**, *119*, 17480.

[46] J. Gao, J. C. Johnson, *ACS Nano* **2012**, *6*, 3292.

[47] C. H. M. Chuang, A. Maurano, R. E. Brandt, G. W. Hwang, J. Jean, T. Buonassisi, V. Bulović, M. G. Bawendi, *Nano Lett.* **2015**, *15*, 3286.

[48] S. Kahmann, M. Sytnyk, N. Schrenker, G. J. Matt, E. Spiecker, W. Heiss, C. J. Brabec, M. A. Loi, *Adv. Electron. Mater.* **2018**, *4*.

[49] S. Jin, Y. Zheng, A. Li, *J. Appl. Phys.* **1997**, *82*, 3870.

[50] M. S. Gaponenko, A. A. Lutich, N. A. Tolstik, A. A. Onushchenko, A. M. Malyarevich, E. P. Petrov, K. V Yumashev, *Phys. Rev. B.* **2010**, *82*, 1.